

# Quantum Monte Carlo calculations of structural properties of FeO under pressure

Jindřich Koloreň\* and Lubos Mitas

*Department of Physics and CHiPS, North Carolina State University, Raleigh, North Carolina 27695, USA*

(Dated: October 27, 2018)

We determine the equation of state of stoichiometric FeO employing the diffusion Monte Carlo method. The fermionic nodes are fixed to those of a wave function having the form of a single Slater determinant. The calculated ambient pressure properties (lattice constant, bulk modulus and cohesive energy) agree very well with available experimental data. At approximately 65 GPa, the lattice structure is found to change from rocksalt type (B1) to NiAs based (inverse B8).

PACS numbers: 72.80.Ga, 71.15.-m, 71.20.-b, 64.30.+t

Transition metal oxides are solids with strong electron-electron correlations that lead to a rich variety of observed structural and electronic phases. Almost all transition metal oxides are a problem on its own due to competitive interplay among correlation and exchange in  $d$ -subshells, crystal fields,  $d$ - $p$  hybridization and charge transfer. Elucidation of high-pressure properties of FeO is of particular interest in geophysics, since this compound belongs to constituents of the deep Earth's interior. FeO is also one of the challenging simple oxides due to the nominally open-shell occupation of the  $3d$  levels. Indeed, this system proved to be problematic for the density functional theory (DFT) in its local density or generalized gradient approximations (LDA or GGA). For example, both LDA and GGAs predict an incorrect ground state lattice structure [1, 2, 3].

At ambient conditions, FeO crystallizes in B1 (NaCl-type) structure. It is antiferromagnetically ordered at temperatures below 198 K and this ordering is accompanied by a small rhombohedral distortion denoted as rB1—the unit cell is stretched along the [111] body diagonal. In shock-wave studies it was observed that around 70 GPa the oxide transforms to a different structure [4], which was inferred as B2 (CsCl-type) in analogy with similar materials, but LDA calculations hinted that much larger pressure, around 500 GPa, would be needed to stabilize B2 against the B1 phase [5]. Besides that, no such structural transition was detected in static compression experiments [6], unless the material was significantly heated up [7]. X-ray diffraction performed along the high-temperature static compression revealed that the high-pressure structure is actually B8 (NiAs-type) [7].

There are two distinct ways of putting FeO on NiAs lattice, the so-called normal B8, where iron occupies Ni sites, and inverse B8 (iB8 for short), where iron sits on As sites. It is the latter configuration that comes from band-structure theories as the more stable of the two [1, 2, 3]. Also, reinterpretation of the data of Ref. 7 suggests that the high pressure phase is a mixture of B8 and iB8 phases [1]. On the theoretical side, the introduction of the iB8 structure into the picture revealed a serious deficiency in the LDA (and GGA) as applied to FeO, since the iB8 phase is predicted more stable not only than B8 but also

than B1 at all pressures, which contradicts experimental findings. It was demonstrated that inclusion of Coulomb  $U$  to better account for electron-electron correlations alleviates this problem [2, 3].

In this Letter, we calculate the equation of state of stoichiometric FeO using the fixed-node diffusion Monte Carlo method (DMC) [8], a many-body computational technique that accurately treats even strongly correlated systems. Based on the aforementioned studies, we confined ourselves to only two structures—B1 with the type-II antiferromagnetic (AFM) ordering (symmetry group  $R\bar{3}m$ ) and iB8 also in the AFM state (group  $P\bar{6}m2$ ). We show that DMC, even in its simplest version based on a single-determinant Slater–Jastrow wave function, provides a very consistent picture of this complicated system that closely follows experimental data including estimation of the transition pressure.

The guiding wave function that defines (fixes) the fermionic nodes in our DMC simulations is of the Slater–Jastrow type  $\Psi_G = \Psi_S \exp[J]$ , where

$$\Psi_S(\mathbf{r}_1, \dots, \mathbf{r}_N) = \det\{\psi_\sigma\} = \det\{\phi_\alpha^\uparrow\} \det\{\phi_\beta^\downarrow\}, \quad (1a)$$
$$J(\mathbf{r}_1, \dots, \mathbf{r}_N) = \sum_{i,j} f(\mathbf{r}_i - \mathbf{r}_j) + \sum_{i,I} g(\mathbf{r}_i - \mathbf{R}_I). \quad (1b)$$

The lower-case indices in Eq. (1b) run over electrons, while the upper-case index denotes ions. The Jastrow correlation factor  $J$  contains one- and two-body terms,  $g$  and  $f$ , that have the same form as in Ref. 9 and represent 17 variational parameters that were optimized within variational Monte Carlo (VMC) framework. The single determinant of spinorbitals  $\psi_\sigma$  becomes a product of spin-up and -down determinants of spatial orbitals  $\{\phi_\alpha^\uparrow, \phi_\beta^\downarrow\}$  after fixing the electron spins,  $N^\uparrow = N^\downarrow = N/2$ , while the overall state is a spin-unrestricted antiferromagnet.

The large energy scale of core electrons poses a difficulty to the DMC in an analogous way as it does to plane-wave based electronic structure techniques. Therefore, we replace the atomic cores by norm-conserving pseudopotentials [10] within the so-called localization approximation [11]. We utilize only small-core pseudopotentials to minimize losses in accuracy as much as possible. We

have argued recently [12] that even small-core pseudopotentials could lead to imprecisions in description of transition metal compounds if a spin-related transition occurs as a part of the phenomena of interest. However, it should not affect the present calculations, since iron atoms in FeO stay in a high-spin state in the whole range of pressures we study in both B1 and iB8 phases. This applies to the DMC results as well as to the flavors of DFT that we used to construct the Slater determinants.

The quality of the fixed-node DMC total energy is determined solely by the quality of fermionic nodes of the guiding wave function. When the form of Eq. (1) is adopted, the parameters controlling location of fermionic nodes are the one-electron orbitals  $\{\phi_\alpha, \phi_\beta\}$ . The direct VMC optimization of these orbitals is currently impractical for simulation sizes required in the present study. Instead, we use one-electron orbitals from spin-unrestricted calculations with hybrid PBE0 functional given as [13]

$$E_{xc}^{PBE0} = aE_x^{HF} + (1-a)E_x^{PBE} + E_c^{PBE}. \quad (2)$$

Here  $E_x^{PBE}$  and  $E_c^{PBE}$  are exchange and correlation parts of the PBE-GGA [14],  $E_x^{HF}$  is the exact exchange from Hartree-Fock (HF) theory and the weight  $a$  is in the range  $0 < a < 1$ . We have found that the inclusion of exact exchange term into PBE-GGA has similar effect as Coulomb  $U$  in the LDA+ $U$  method. It opens a gap in the electronic spectrum of the AFM B1 phase and stabilizes it relative to the iB8 structure. Both the gap and the transition pressure increase with increasing  $a$ . With mixing weight  $a = 0.05$ , the iB8 is still more stable than B1 everywhere, the B1 to iB8 transition occurs at 5 GPa for  $a = 0.1$  and at 43 GPa for  $a = 0.2$ . Note that in MnO, which exhibits similar structural transition, the experimental range of transition pressures is reached already for  $a \approx 0.1$  [12], while in the present case of FeO, the transition takes place much sooner than in experiments ( $\geq 70$  GPa) even for twice as much exact-exchange content in PBE0.

The exchange-correlation functional of Eq. (2) defines one-parametric class of single-particle orbitals  $\{\phi_\alpha^{(a)}, \phi_\beta^{(a)}\}$ , which can be used to minimize the DMC fixed-node error by varying the exact exchange weight  $a$ . Although in simple insulators, such as silicon, the differences between fixed-node energies corresponding to various sets of one-particle states were found to be rather marginal [15], more pronounced differences have been obtained for transition metal compounds. In isolated molecules of transition metal monoxides, the fixed-node DMC energies with orbitals from B3LYP (hybrid functional similar to PBE0) are noticeably lower than with HF or pure DFT orbitals [9, 16]. DMC optimization of the exact exchange proportion in the B3LYP was performed in Ref. 16 for the MnO molecule. The optimal value was reported as approximately 17%, but the minimum was rather broad and shallow and values between 5% and 30% were almost equivalent. Therefore,

we have chosen the weight  $a$  in PBE0 to be  $a = 0.2$ , corresponding to 20% of GGA exchange being replaced with the exact exchange. In the following we abbreviate this functional as PBE0<sub>20</sub>. This choice is compatible with findings of Ref. 16 and leads to reasonable ambient-pressure properties of FeO already within (hybrid) DFT, i.e., B1 structure is insulating and more stable than iB8. We also checked that at equilibrium the PBE0<sub>20</sub> orbitals provide DMC energy 0.3 eV per FeO lower than orbitals from the HF approximation.

In our simulations, the infinite crystal was modelled by a periodically repeated simulation cell containing 8 FeO units, i.e., 176 valence and semi-core electrons. Although such a system is certainly not small to deal with in an explicitly many-body fashion, it turns out that finite-size effects are significant if not treated properly. The origin of these finite-size errors is twofold. One part is related to incorrect momentum quantization due to confinement of electrons into the simulation cell, the second part comes from the artificial periodicity of exchange-correlation hole due to periodic extension of Coulomb potential using the Ewald summation.

The problem associated with confinement appears also in mean-field band theories, where it is exactly resolved by integration over the first Brillouin zone, while working only within the smallest “simulation” cell possible, the primitive cell. Each  $\mathbf{k}$ -point in the first Brillouin zone corresponds to a different boundary condition imposed on the primitive cell. The momentum integration is equivalent to averaging over these so-called twisted boundary conditions. Analogous averaging procedure performed in a many-body simulation does not represent a complete correction, but it proved to be very efficient within Monte Carlo algorithms [17]. In this study we deal only with insulating states, which simplifies matters considerably and we have found that just 8 twists are enough for our simulation cell size. We have verified that within PBE0<sub>20</sub> the total energy obtained in our simulation cell using just 8  $\mathbf{k}$ -points differs only  $\approx 0.01$  eV per FeO from fully converged integral over Brillouin zone.

The second part of finite-size errors, originating from artificial periodicity of the Ewald potential, is accounted for with the aid of the correction introduced in Ref. 18. The estimate for the energy at infinite volume is written as

$$E = E_{Ewald} + \frac{1}{4\pi^2} \int_D d^3k \frac{S(\mathbf{k})}{k^2}. \quad (3)$$

The static structure factor is defined as  $S(\mathbf{k}) = \langle \Psi_0 | \hat{\rho}_{\mathbf{k}} \hat{\rho}_{-\mathbf{k}} | \Psi_0 \rangle / N$  with  $\hat{\rho}_{\mathbf{k}}$  standing for a Fourier component of the electron density. The integral in Eq. (3) runs over a domain  $D$  centered around  $\mathbf{k} = 0$  and having volume  $8\pi^3/\Omega$ , where  $\Omega$  is volume of the simulation cell. The structure factor  $S(\mathbf{k})$  is evaluated within the DMC at a discrete set of points and then extrapolated towards  $\mathbf{k} = 0$ . Performance of the correction given by

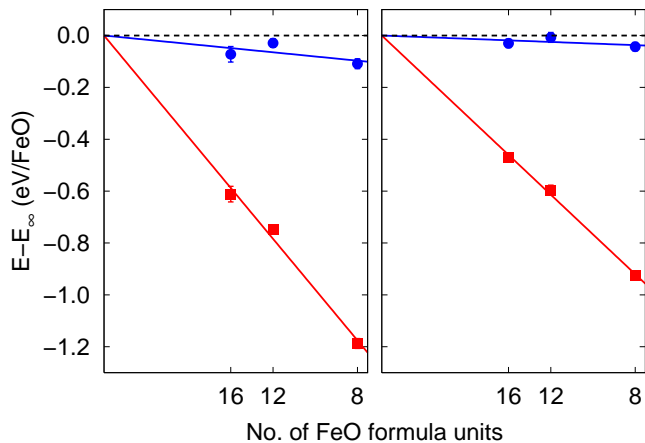


FIG. 1: (color online) Finite-size errors of the twist averaged DMC energy at volumes  $15.9 \text{ \AA}^3/\text{FeO}$  (left) and  $20.4 \text{ \AA}^3/\text{FeO}$  (right). Pure Ewald energies are shown as red squares, values corrected according to Eq. (3) are represented by blue circles. Note that the finite-size errors increase with increasing the electron density. The energy in infinite cell  $E_\infty$  is extrapolated from the data shown. Statistical errorbars are smaller than symbol sizes except for the largest cell in the left panel.

Eq. (3) applied to FeO is illustrated in Fig. 1, where we plot the total energy at two different electron densities as calculated in simulation cells of varied size up to 16 FeO units, i.e., 352 valence and semi-core electrons. The correction removes more than 90% of the finite-size error introduced by the periodic electron-electron interaction potential and enables us to replace expensive size scaling analysis of Fig. 1 by a simple formula, Eq. (3).

*Results.* First we discuss properties of the B1 phase around equilibrium volume. For the cohesion energy,  $E_{coh} = E_{Fe} + E_O - E_{FeO}$ , our DMC simulations yield  $9.66 \pm 0.04 \text{ eV/FeO}$  that matches  $9.7 \text{ eV/FeO}$  deduced from experimental formation enthalpies [19]. The electronic gap, which we calculate as a difference between total energies of the ground state and the first excited state at the  $\Gamma$ -point in our 8 FeO simulation cell, comes out as  $2.8 \pm 0.3 \text{ eV}$ . This value is not too far from optical absorption edge observed near  $2.4 \text{ eV}$  [20]. The weak feature displayed between 1.0 and 1.5 eV in these experiments is not reproduced in the picture of FeO we present here. However, it is quite possibly related to imperfections in structural or magnetic order, since essentially the same absorption band was repeatedly observed in other systems where Fe atoms act as impurities [21, 22].

The DMC energy as a function of volume, together with fitted Murnaghan equation of state, is presented in Fig. 2. The parameters of the least-square fit are compared with predictions of other electronic structure methods and with experiments in Tab. I. The DMC estimate for equilibrium lattice constant  $a_0$  is in excellent agreement with experimental value extrapolated to stoichiometric FeO and offers more consistent prediction than

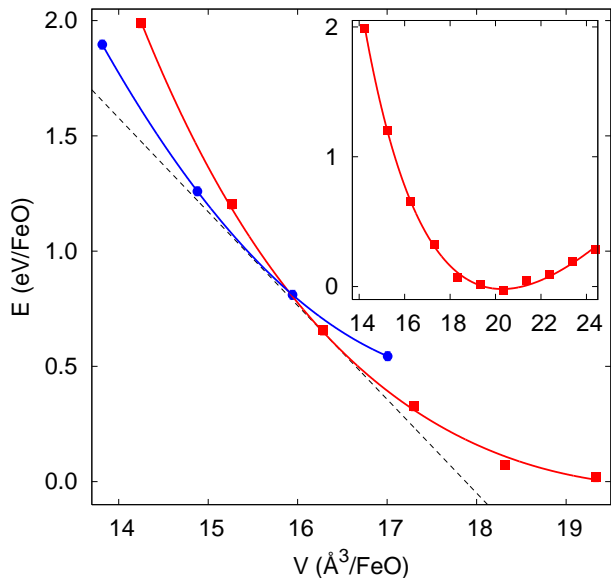


FIG. 2: (color online) Total energies of B1 (red squares) and iB8 (blue circles) phases. Statistical errorbars are smaller than symbol sizes. Lines are least-square fits with Murnaghan equation of state. The dashed double tangent corresponds to the transition pressure of 65 GPa. Inset shows the data for B1 phase over wider volume region, including equilibrium.

LDA or GGA. On the other hand, the hybrid PBE0<sub>20</sub> functional, which we used to construct the DMC guiding wave function, provides a similar value. All methods shown in Tab. I provide essentially the same value of bulk modulus, which is noticeably larger than typical experimental reports. The extrapolation to stoichiometry is, however, expected to lead to values in the vicinity of the theoretical data [23, 24]. The isothermal pressure derivative of the bulk modulus,  $K'_0$ , turns out to be larger in DMC than in the density-functional approaches, which makes it compatible with elastic-wave experiments [24].

The equation of state calculated within diffusion Monte Carlo up to large hydrostatic pressures is shown in Fig. 2.

TABLE I: Equilibrium lattice constant  $a_0$ , bulk modulus  $K_0$  and its derivative  $K'_0 = (\partial K_0 / \partial P)_T$  calculated in this work (DMC and PBE0<sub>20</sub>) compared to selected theories and experiments. The experimental lattice constant is extrapolated to the stoichiometric FeO, whereas the values of  $K_0$  and  $K'_0$  are not. The extrapolated value of bulk modulus  $K_0$  is estimated around 180 GPa [23, 24].

	$a_0$ (Å)	$K_0$ (GPa)	$K'_0$
DMC	4.324(6)	170(10)	5.3(7)
PBE0 <sub>20</sub>	4.328	182	3.7
GGA [3]	4.28	180	3.6
LDA [5]	4.136	173	4.2
experiment	4.334 [23]	152.3 [24]	4.92 [24]

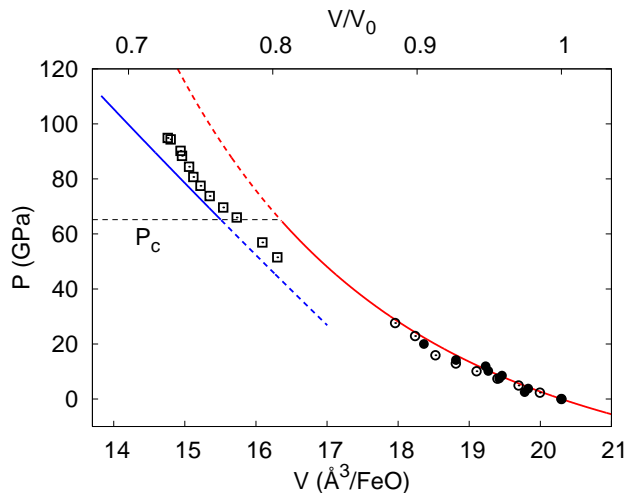


FIG. 3: (color online)  $P(V)$  curves of B1 (red) and iB8 (blue) phases. Lines are our DMC fits as in Fig. 2. Points are experimental data: filled circles [6] (B1,  $\text{Fe}_{0.98}\text{O}$ ), empty circles [28] (B1,  $\text{Fe}_{0.94}\text{O}$ ), empty squares [7] (iB8,  $\text{Fe}_{0.98}\text{O}$ ). All B1 data [6, 28] were taken at room temperature, the iB8 data [7] correspond to 900 K. B1 datasets are shown relative to the equilibrium volumes reported in the individual studies to approximately remove the non-stoichiometry effects.

The  $c/a$  ratio in the hexagonal iB8 phase, stable at high pressures, was optimized within PBE0<sub>20</sub>. It was found to increase from 1.93 at volume 17  $\text{\AA}^3/\text{FeO}$  to 2.03 at 14  $\text{\AA}^3/\text{FeO}$ . These ratios agree well with experimental  $c/a = 2.01$  at 14.83  $\text{\AA}^3/\text{FeO}$  reported in Ref. 7.

The B1 phase, stable at low pressures, was assumed cubic, i.e., we neglected the rhombohedral distortion. We did not use the DFT optimized geometries in this case, because DFT based techniques are not conclusive in determination of the rhombohedral distortion [25, 26, 27]. We checked the impact of fixing the cubic symmetry by comparing DMC total energies for different distortions at high compression, where the distortion has the largest impact. At the volume of 15.3  $\text{\AA}^3/\text{FeO}$ , the energy gain associated with the rhombohedral distortion was of the order of statistical errorbars  $\approx 0.02$  eV/FeO, i.e., too small to affect the results.

The critical pressure  $P_c$  of the structural transition from B1 to iB8 phase was determined from equality of Gibbs potentials,  $G_{B1}(P_c) = G_{iB8}(P_c)$ , graphical equivalent of which—the double tangent—is shown in Fig. 2. The value is  $P_c = 65 \pm 5$  GPa with the errorbar given by statistical fluctuations of the Monte Carlo simulations. The prediction  $P_c = 65$  GPa agrees quite well with shock-wave data and with high-temperature static compression experiments, except for the fact that our investigation is performed at  $T = 0$ , for which experiments suggest considerably higher transition pressure. Our finding could be interpreted as an indirect support for existence of an energy barrier between the two phases that requires a thermal activation to be overcome.

Another means of comparison with experiments is looking at the  $P(V)$  equation of state, Fig. 3. Agreement between data for B1 structure (after extrapolation to stoichiometric FeO) is very good, which is in concord with similarly good correspondence of ambient pressure parameters compared in Tab. I. Our curve for iB8 structure also follows the x-ray data of Ref. 7 rather nicely (no stoichiometry related correction was attempted in this case). Experimentally, this phase is perhaps somewhat stiffer than in our calculations, which signals that DMC is likely to slightly underestimate the transition pressure  $P_c$ .

*In summary*, the equation of state and basic electronic structure of FeO calculated with the diffusion Monte Carlo agrees very well with many aspects of available experimental data. Considering that the DMC is essentially a parameter-free method and that the fixed-node condition was enforced with the aid of a very simple wave function (single Slater determinant), the degree of consistency of the provided picture is quite remarkable.

We acknowledge support by NSF DMR-0121361 and EAR-0530110 grants. This study was enabled by INCITE allocation at ORNL and by allocation at NCSA. QMC simulations were done using QWALK code [29], and the one-particle orbitals were calculated with CRYSTAL2003 [30].

\* On leave from Institute of Physics, Academy of Sciences of the Czech Republic, Na Slovance 2, CZ-18221 Praha 8, Czech Republic; kolorenc@fzu.cz

- [1] I. I. Mazin, et al., *American Mineralogist* **83**, 451 (1998).
- [2] Z. Fang, et al., *Phys. Rev. Lett.* **81**, 1027 (1998).
- [3] Z. Fang, et al., *Phys. Rev. B* **59**, 762 (1999).
- [4] R. Jeanloz et al., *Geophys. J. R. Astr. Soc.* **62**, 505 (1980).
- [5] D. G. Isaak, et al., *Phys. Rev. B* **47**, 7720 (1993).
- [6] T. Yagi, et al., *J. Geophys. Res.* **90**, 8784 (1985).
- [7] Y. Fei et al., *Science* **266**, 1978 (1994).
- [8] W. M. C. Foulkes, et al., *Rev. Mod. Phys.* **73**, 33 (2001).
- [9] L. K. Wagner et al., *J. Chem. Phys.* **126**, 034105 (2007).
- [10] Y. Lee, private communication, see also Y. Lee, et. al, *Phys. Rev. B* **62**, 13347 (2000) for large core version of these pseudopotentials.
- [11] L. Mitáš, et al., *J. Chem. Phys.* **95**, 3467 (1991).
- [12] J. Kolorenc et al., *Phys. Rev. B* **75**, 235118 (2007).
- [13] J. P. Perdew, et al., *J. Chem. Phys.* **105**, 9982 (1996).
- [14] J. P. Perdew, et al., *Phys. Rev. Lett.* **77**, 3865 (1996).
- [15] P. R. C. Kent, et al., *Phys. Rev. B* **57**, 15293 (1998).
- [16] L. Wagner et al., *Chem. Phys. Lett.* **370**, 412 (2003).
- [17] C. Lin, et al., *Phys. Rev. E* **64**, 016702 (2001).
- [18] S. Chiesa, et al., *Phys. Rev. Lett.* **97**, 076404 (2006).
- [19] D. R. Linde, ed., *CRC Handbook of Chemistry and Physics* (CRC Press/Taylor and Francis, 2007).
- [20] H. K. Bowen, et al., *J. Solid State Chem.* **12**, 355 (1975).
- [21] G. D. Jones, *Phys. Rev.* **155**, 259 (1967).
- [22] A. Hjortsberg, et al., *Phys. Rev. B* **37**, 3196 (1988).
- [23] C. A. McCammon et al., *Phys. Chem. Minerals* **10**, 106

- (1984).
- [24] I. Jackson, et al., *J. Geophys. Res.* **95**, 21671 (1990).
- [25] M. Cococcioni et al., *Phys. Rev. B* **71**, 035105 (2005).
- [26] S. A. Gramsch, et al., *American Mineralogist* **88**, 257 (2003).
- [27] W.-B. Zhang, et al., *Solid State Commun.* **142**, 6 (2007).
- [28] R. L. Clendenen et al., *J. Chem. Phys.* **44**, 4223 (1966).
- [29] L. K. Wagner, et al., arXiv:0710.4361, [www.qwalk.org](http://www.qwalk.org).
- [30] V. Saunders, et al., *CRYSTAL2003 User's Manual* (University of Torino, Torino, 2003).